optica

Non-invasive light focusing in scattering media using speckle variance optimization: supplementary material

ANTOINE BONIFACE[1,*], BAPTISTE BLOCHET[1,2], JONATHAN DONG[1,3], AND SYLVAIN GIGAN[1]

[1] Laboratoire Kastler Brossel, Sorbonne Université, École Normale Supérieure–Paris Sciences et Lettres (PSL) Research University, CNRS, Collège de France, 24 rue Lhomond, 75005 Paris, France

[2] IBENS, Département de Biologie, Ecole Normale Supérieure, CNRS, Inserm, PSL Research University, F-75005 Paris, France

[3] Laboratoire de Physique de l'École Normale Supérieure, Université PSL, CNRS, Sorbonne Université, Université Paris-Diderot, Sorbonne Paris Cité, Paris, France

[*] Corresponding author: antoine.boniface@lkb.ens.fr

Published 23 October 2019

This document provides supplementary information to "Non-invasive light focusing in scattering media using speckle variance optimization," https://doi.org/10.1364/OPTICA.6.001381.

A. Variation of the spatial standard deviation with respect to Φ

Below we derive the theoretical variation of the variance with respect to the phase Φ of a given SLM segment/input mode. We denote $I_{fluo}(x,y)$ the 2-dimensional fluorescent speckle intensity in the imaging plane. I_{fluo} is the incoherent sum of all the speckles generated by each individual target: $I_{fluo}(x,y,\Phi) = \sum I_{exc}^{(k)}(\Phi) i_k(x,y)$, where:
· $i_k(x,y)$ is the spatial shape of the speckle emitted by the k^{th} target.
· $I_{exc}^{(k)}(\Phi) = a_k \sin(\Phi+\theta) + c_k$ corresponds to the intensity of the illumination speckle on target k.
Then the variance of the fluorescent speckle, $\mathrm{Var}(I_{fluo}(x,y,\Phi))$ reads:

$$
\begin{aligned}
\mathrm{Var}(I_{fluo}(x,y,\Phi)) &= \mathrm{Var}(\textstyle\sum I_{exc}^{(k)}(\Phi) i_k(x,y)) \\
&= \textstyle\sum I_{exc}^{(k)}(\Phi)^2 \mathrm{Var}(i_k(x,y)) \\
&= \textstyle\sum (a_k \sin(\Phi+\theta) + c_k)^2 \mathrm{Var}(i_k(x,y)) \\
&= \textstyle\sum (a_k^2 \sin^2(\Phi+\theta) + 2a_k c_k \sin(\Phi+\theta) + c_k^2) \mathrm{Var}(i_k(x,y)) \\
&\equiv A \sin(2\Phi + \theta_A) + B \sin(\Phi + \theta_B) + C
\end{aligned}
\tag{S1}
$$

where A, θ_A, B, θ_B and C are constants.

We explicitly see that the non-linearity introduced by the variance is of order 2. By comparison, the total 2-photon intensity, $I^{2p}(\Phi) = \sum \lambda_k^2(\Phi)$, presents the same evolution with respect to Φ. This explains why using the spatial variance of a linear signal as a feedback enables us focusing light on a single target, like in 2-photon optimization.

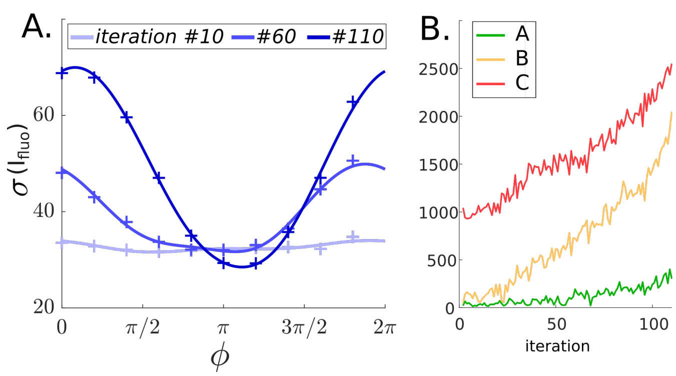

Fig. S1. A. Fit of standard deviation experimental data for three different Hadamard modes. **B**. Evolution of the corresponding fitting coefficients throughout the optimization.

In Fig.S1.A we validate our model and show that standard deviation experimental data, $\sigma(I_{fluo})$, fit well with $\sqrt{eq.(S1)}$. These curves also highlight the non-linearity of order 2 that is predominant for the first iterations (iteration #10 and #60). After a higher number of iteration, the fluorescence that we capture is predominantly emitted by a single target, which explains the sinusoidal shape (iteration #110).

Additionally, we look into the contribution of second and first order term in (S1), coefficient A and B respectively (Fig.S1.B). The first iterations are the most non-linear ones with respect to Φ: coefficients A and B are of the same order. Then, B is increasingly larger than A, which is consistent with the fact that the optimization mainly increases the total intensity rather than the contrast. This theoretical model can also be used to estimate with higher accuracy the phase that maximizes the variance. This phase is estimated by performing N_{step} discrete measurements (corresponding to N_{step} different SLM phase masks). Our model (eq. (S1)) contains 5 independent parameters which imposes a minimal value for N_{step} to correctly fit our experimental data. But after only few tens of iterations the coefficient A corresponding to the second order term is small compare to the first order one B. Therefore our fitting function can be approximated to $\sigma(I(x,y,\Phi)) \simeq \sqrt{(B\sin(\Phi+\theta_B)+C)}$. Now we only need to determine 3 parameters, allowing us to decrease N_{step}, which speeds up the optimization procedure.

B. Experimental limitations

In this part we study in more details the limits of our focusing approach. We have done complementary numerical simulations where we can easily adjust the level of noise. An appropriate model has also been derived to describe the results.

One necessary condition required by our technique is that the variance modulation depth with respect to the phase of the input mode must be detectable. Otherwise, the phase that maximizes the variance is not correctly measured and the metric is not optimized. The critical step in ensuring the convergence of the algorithm is the optimization of the first modes; at the beginning of the optimization, the contrast of the fluorescent speckle can indeed be quite low. The latter depends essentially on:

- the beads (size and number of excited beads, spectral emission bandwidth of the fluorescence)

- the scattering medium (spectral correlation bandwidth, speckle grain size / size of the bead)

Qualitatively, the reason why the contrast remains measurable even for many beads and relatively scattering situation, is the very mild decrease in speckle contrast, when summing incoherently speckle pattern. Indeed, for N incoherently summed speckle patterns, the contrast is $1/\sqrt{N}$. For example, summing 100 speckle patterns still results in a contrast of 0.1, easily measurable even under high noise level.

In the following, we investigate more quantitatively the robustness of our approach with respect to noise. The noise may essentially come from fluorescence generated outside the beads (for instance auto-fluorescence of parafilm) and detector noise (dark and shot noise).

The procedure is the following: (1) we run numerical simulations and (2) we compare the results with a qualitative model.

(1) Numerical Simulations

Our simulation consists in reproducing, to some extent, our experimental protocol in order to study the theoretical limits of our optmization method. More particularly, we look into the influence of the contrast of the fluorescent speckle emitted by a single source, denoted C_{target}, versus an additive gaussian noise. While this by no means correctly simulates all type of noise present in the experiment, we believe it is sufficient to get a better understanding of the limits of our techniques.

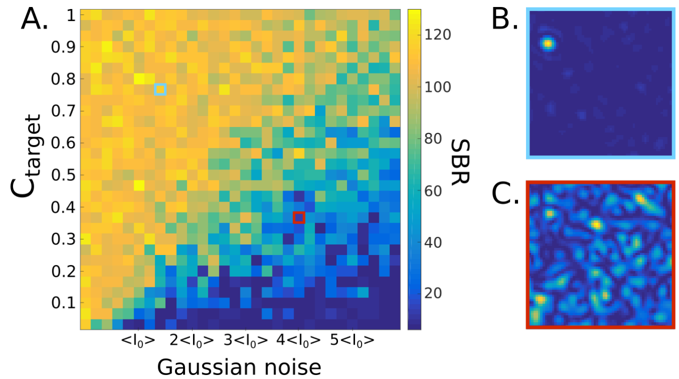

Fig. S2. Robustness of our variance-based method with respect to noise. **A**. Signal-to-background ratio map as a function of the contrast and noise levels. A high SBR means that the variance optimization technique has been successful. In order to consistently form a focus our technique needs to correctly estimate the variance modulation of the fluorescent speckle emitted by the beads. This requirement sets a trade-off between the contrast of the speckle emitted by a single target and the surrounding noise. A linear trend is observed: if C_{target} is high enough with respect to noise the illumination is focused on a single target as in **B**. (SBR = 108.9), otherwise the optimization fails, **C**. (SBR = 12.3).

a. Model

Our numerical model optimizes the phase of $N_{SLM} = 256$ SLM segments over $N_{iter} = 400$ iterations. The number of targets is set to $N_{target} = 3$. We only tune 2 parameters:

- the contrast of the fluorescent speckle emitted by a single bead, denoted C_{target}. Experimentally it would correspond to tune either $\Delta\lambda$, the spectral bandwidth of the fluorescence emitted by the beads or $\delta\lambda_m$, the spectral bandwidth of the scattering medium. Note that in the multiply scatterin regime, the spectral bandwidth is proportional to $\delta\lambda_m \propto l_t/L^2$, where l_t is the transport mean free path and L the thickness of the medium.

- the noise level. We numerically consider an additive gaussian noise scaled on the average intensity of the initial fluorescent speckle, $\langle I_0 \rangle$.

In our numerical simulations, we generate the transmission matrices from complex random matrices.

b. Results

For each set of values {contrast + noise} we run 5 realizations for 5 different transmission matrices. We report in Fig.S2 the mean value over the 5 realizations.

Convergence of our iterative method is quantified with the signal-to-background ratio (SBR) of the focus we may form. These numerical results show that our variance-based optimization technique succeeds well even if the initial contrast is very low. As one can see, as long as we have no noise in our system a focus is always formed. Otherwise, the noise level determines the minimal required value for C_{target} to get a focus. This requirement also depends on the number of excited targets. If the number of targets increases, the overall contrast is reduced which restricts the applicability of our technique.

(2) Comparison with a qualitative model

We propose a simple model to explain the trend of these numerical results. During the optimization process, we need to estimate the variance of the fluorescent speckle. This estimation is corrupted by noise. We can derive scaling laws of the regions of parameters in which the algorithm is successful.

We denote by C_{target} the contrast of the fluorescent speckle emitted by a single target and I its average intensity. The variance of this fluorescent speckle is $C_{target}^2 \times I^2$, and when several independent speckle patterns are summed, the corresponding variance is equal to $N \times C_{target}^2 \times I^2$.

On the other hand, the mean intensity is equal to $N \times I$ and with multiplicative gaussian noise of amplitude b, the variance originating from noise fluctuations between different pixels of the camera scales as $b^2 \times N^2 \times I^2$.

Hence, we compare $N \times C_{target}^2 \times I^2$ and $b^2 \times N^2 \times I^2$, which gives a scaling $b \sim C_{target}/\sqrt{N}$. Light focusing is thus achievable only if the noise level is low compared to the initial contrast of the individual speckle patterns. This linear scaling is well-verified in the numerical simulations, meaning that the main criterion for the optimization to succeed is that the variance needs to be correctly estimated in the first steps of the optimization.

C. Performances in more demanding regimes

(1) With a larger number of beads

To show the strength and limitations of our technique, we increase the number of beads in our fluorescent sample. In particular, we show that focusing is still achievable up to a certain limit. In Fig.S3.A. we have 43 fluorescent beads, and as one can see the optimization procedure still consistently converge to a single diffraction-limited focus.

Nevertheless, if the sample contains a much larger number of beads (>200) with clusters (see Fig.S3.B) the illumination tends to form an extended focus. With such a number of fluorophores, the initial contrast is very low and the optimization seems to mainly enhance the contrast of the envelope ($C(I_{center})$ hardly increases, Fig.S3.C), thus focusing light on an extended area. However, this does not mean that our technique fails. An increase in standard deviation is noticeable. In this regime, the initial contrast can be enhanced by using a bandpass filter and/or an analyser at the cost of fluorescence signal.

(2) With a thicker scattering medium

In order to show that 3 layers of parafilm is by no means the ultimate limit, we have repeated the experiment with 6 layers of parafilm (corresponding to $4-5l_s$ and $1l_t$) and for $\simeq$ 20 beads. In Fig.S4 we report experimental data obtained before and after variance optimization. It proves that our variance-based method is still efficient in this kind of regime. Note that for this experiment only, we have replaced the objective 50x, NA 0.75 (placed in transmission) by a 20x, NA 0.4 in order to have a larger field of view to recover all the speckle.

D. Scattering properties of parafilm

Parafilm is a widespread scattering medium in order to mimic qualitatively the scattering properties of static biological tissues. In particular it shows very little ballistic and has a lot of forward scattering. It is also cheap and easy handling. However, its optical scattering properties have not been studied yet. In order to be more quantitative, we report in this subsection additional measurements to fully characterize the scattering properties of the medium. Note that all measurement were performed at 532nm.

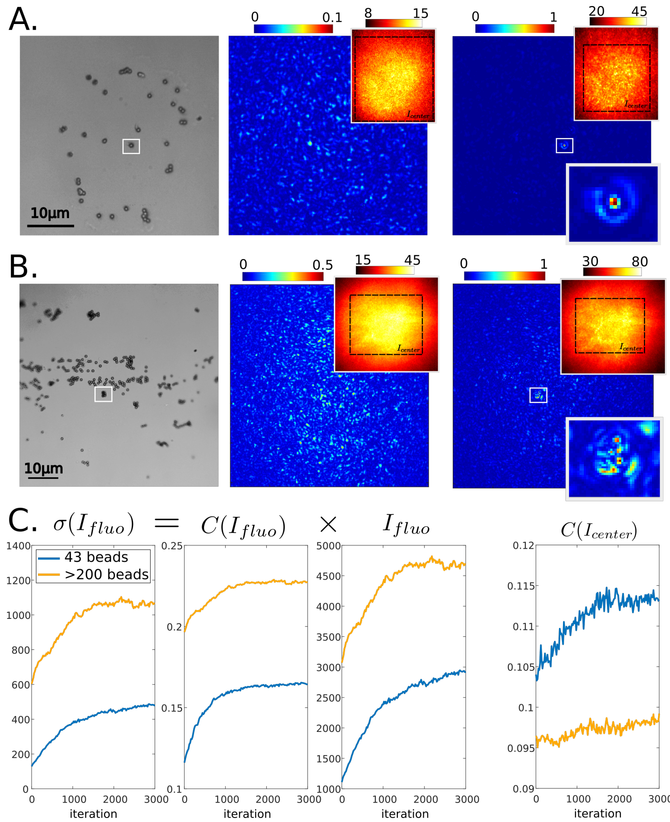

Fig. S3. Influence of the number of beads. **A**. With 43 beads a focus is still formed at the end of the variance optimization. However when the number of targets becomes too large (**B**) and the density increases, although the variance can still be optimized, as seen in (**C**), a focus is not always formed.

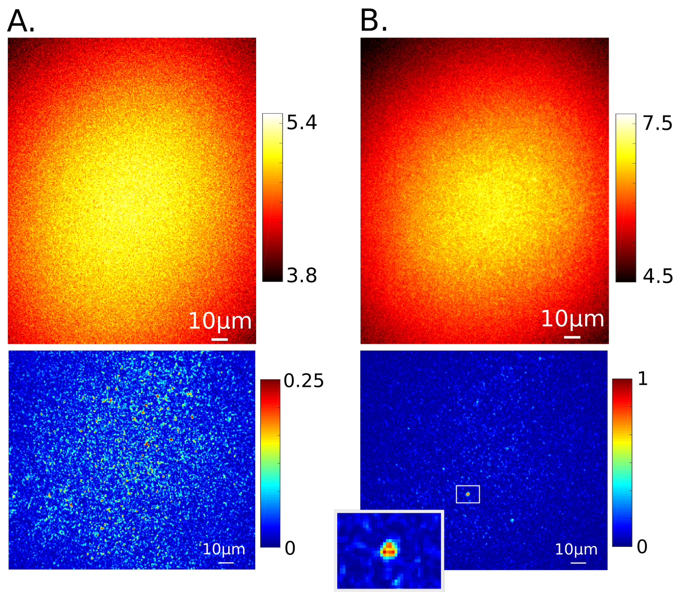

Fig. S4. Light focusing on one over $\simeq$ 20 possible beads through 6 layers of parafilm. **A**. Before optimization Top: fluorescent speckle on CAM1. Bottom: speckle illumination in the plane of the beads, CAM2. **B**. After the optimization of $N_{iter} = 800$ iterations.

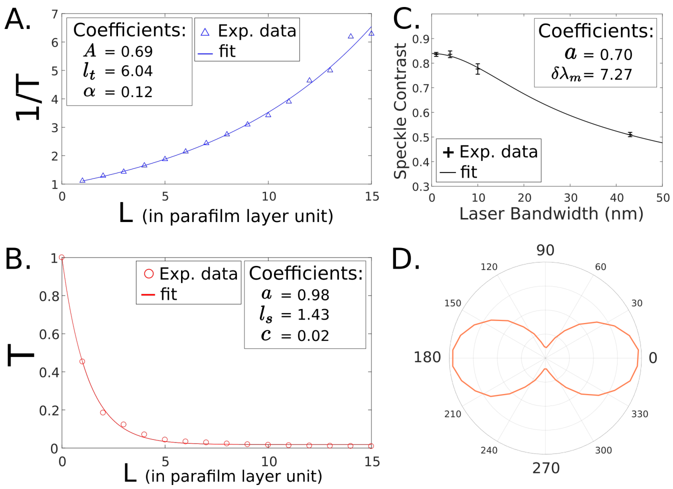

Fig. S5. Properties of parafilm at 532nm. Measurements of : **A**. transport mean free path, l_t - **B**. scattering mean free path, l_s - **C**. spectral correlation bandwidth, $\delta\lambda_m$ (3 layers of parafilm) - **D**. output polarization diagram of light after passing through 3 layers of parafilm.

First we measured its transport mean free path in Fig.S5.A. The measurement of the total transmission T is made by placing an integrating sphere (FOIS-1, Ocean Optics) at the output face of the scattering medium. We detect the signal with a large area photodiode and an oscilloscope. We repeated this measurement for various thicknesses and then extract the transport mean free path from a fit. The thickness of the medium is changed by adjusting the number of parafilm layers. One layer is $\simeq 120\mu m$ thick. The fitting model is derived from diffusion theory [1]. Note that this model takes into the absorption through the coefficient $\alpha = 1/l_i$, where l_i is the absorption length:

$$T = A\frac{\sinh(2\alpha z_e)\sinh(\alpha z_e)}{\sinh(\alpha(L+2z_e))}$$
$$z_e = \frac{1}{2\alpha}\ln\left(\frac{1+\alpha z_0}{1-\alpha z_0}\right)$$
$$z_0 = 2/3l_t\ln\left(\frac{1+R}{1-R}\right)$$
$$\alpha = 1/l_i$$

The extrapolation length z_e is affected by the internal reflection R via $z_0 = 2/3l_t(1+R)/(1-R)$. Although the analytical expression is rather complex, it has been shown in [2] that $Q = (1+R)/(1-R)$ can be approximated by the polynomial $Q \simeq 504.332889 - 2641.00214n + 5923.699064n^2 - 7376.355814n^3 + 5507.53041n^4 - 2463.357945n^5 + 610.956547n^6 - 64.8047n^7$, where $n = n_1/n_2$, with n_1, n_2 the refractive indices outside and inside the scattering medium, respectively. In our case medium 1 is made of glass $n_1 = 1.44$ and our scattering medium is $n_2 = 1.52$. This leads to $Q \simeq 1.1777$. By injecting this value in our fitting model we can successfully estimate the transport mean free path of parafilm $l_t = 6.04$ parafilm layers, which corresponds approximately to: $l_t \simeq 720\mu m$. This curve allows also to estimate the absorption coefficient $\alpha = 0.12/$ layer, which corresponds to $\alpha \simeq 1mm^{-1}$.

An independent measurement allows us to measure the scattering mean free path, l_s. This is achieved by measuring the transmission of the ballistic light through the sample, Fig.S5.B. In practice we move the objective in transmission far away from the scattering medium and place in between a diaphragm to filter out scattered light. The exponential decay of ballistic photons follows the so-called Beer-Lambert law. The decay is governed by the scattering mean free path and the absorption length and reads:

$$T(z) = a\exp(-(\alpha + 1/l_s)z) + c$$

As for the transport mean free path, we repeat the measurement for various thicknesses. The fitting model gives us $l_s = 1.43$ parafilm layers, which corresponds approximately to: $l_s \simeq 170\mu m$. By comparing l_t and l_s, we can extract the anisotropy factor, here $g = 0.77$, which means that parafilm is highly forward scattering, as expected. Note that these results are relatively similar to the typical scattering properties of biological tissues.

Spectral correlation bandwidth is also a parameter that directly impact the contrast of the speckle. For a spatially coherent source, the speckle contrast is $C = 1/\sqrt{N}$ where N is the number of spectral channels in our system and is defined as $N = \Delta\lambda_{laser}/\delta\lambda_m$, where $\Delta\lambda_{laser}$ is the bandwidth of the laser and $\delta\lambda_m$ the spectral bandwidth of the medium. We refer to [3] for the measurement protocol. We used a supercontinuum source (SC–5–FC, YSL Photonics) and took a subpart of its spectrum around 532nm with 4 different bandpass filters : 1nm, 4nm, 10nm and 43nm. We repeated the measurement at 5 different spatial positions of our sample (made of 3 layers of parafilm) and fitted data in Fig.S5.C with the model we derive below.

In our model, we assume that the spectrum is flat in the range of $\Delta\lambda_{laser} = \lambda_2 - \lambda_1$, the spectral bandwidth determined by the bandpass filter.

We want to compute the variance of the following intensity:

$$I = \int_{\lambda_1}^{\lambda_2} i(\lambda)d\lambda$$

where $i(\lambda)d\lambda$ is an infinitesimal speckle intensity between wavelengths λ and $\lambda + d\lambda$. Each infinitesimal speckle pattern is well-contrasted and has a standard deviation equal to its mean. If we write m the mean of the total intensity, then: $\langle i(\lambda)d\lambda\rangle = \sqrt{\mathrm{Var}(i(\lambda)d\lambda)} = \frac{md\lambda}{\lambda_2-\lambda_1}$ The variance of $i(\lambda)d\lambda$ will also be denoted $v = \frac{m^2d\lambda^2}{(\lambda_2-\lambda_1)^2}$.

The covariance between two different wavelengths λ and λ' is linked with the spectral correlation bandwidth $\delta\lambda_m$: $\mathrm{Cov}(i_\lambda, i_{\lambda'})d\lambda^2 = v.e^{-(\lambda-\lambda')^2/(2\delta\lambda_m^2)}$

We then compute the variance of the integral using Riemann sums, replacing $d\lambda$ by $\frac{\lambda_2-\lambda_1}{N}$ and taking the limit $N\to\infty$. We use the following notation $\gamma = \frac{\lambda_2-\lambda_1}{N}$ and $u = \frac{\lambda_2-\lambda_1}{\delta\lambda_m}$.

$$\begin{aligned}
\mathrm{Var}(I) &= \sum_{j=1}^{N} Var(i(\lambda_1+j\gamma)d\lambda) + 2\sum_{j<k}\mathrm{Cov}(i(\lambda_1+j\gamma), i(\lambda_1+k\gamma)d\lambda^2) \\
&= \sum_{j=1}^{N}\frac{m^2}{N^2} + 2\sum_{j<k}\frac{m^2e^{-(k-j)^2(\lambda_1-\lambda_2)^2/(2\delta\lambda_m^2N^2)}}{N^2} \\
&= \frac{m^2}{N} + \frac{2m^2}{N}\sum_{d=1}^{N-1} e^{-d^2(\lambda_1-\lambda_2)^2/(2\delta\lambda_m^2N^2)}\left(1-\frac{d}{N}\right) \quad ,d = j-k \\
&\to 2m^2\int_0^1 e^{-\frac{(\lambda_1-\lambda_2)^2}{2\delta\lambda_m^2}x}(1-x)dx \quad \text{when} \quad N\to\infty \quad ,x = \frac{d}{N} \\
&= \frac{m^2}{u^2}\left(\sqrt{2\pi}u\,\mathrm{erf}(u\sqrt{2}) + 2e^{-\frac{u^2}{2}} - 2\right)
\end{aligned}$$

The contrast is thus:

$$\begin{aligned} C(u) &= \sqrt{\mathrm{Var}(I)} / \langle I \rangle \\ &= \frac{1}{u}\sqrt{(\sqrt{2\pi}u\,\mathrm{erf}(u\sqrt{2}) + 2e^{-\frac{u^2}{2}} - 2)} \end{aligned}$$

We add a constant multiplicative factor to this equation because the envelope decreases the overall contrast. By fitting our data with the model we previously derived we find for three layers of parafilm a spectral bandwidth $\delta\lambda_m = 7.3nm$. We recall here that for a multiply scattering medium, this bandwidth is known to scale with the inverse of the square thickness of the medium $\delta\lambda_m \propto l_t/L^2$. Therefore we expect the contrast (linked to $\sqrt{\delta\lambda_m}$) to decrease only linearly with the thickness. Note also that with the 43nm bandpass filter (collecting almost all the fluorescence), the contrast is only reduced by a factor 2, thus validating the mild decrease in contrast with respect to the spectral bandwidth.

Another parameter that may affect the contrast of a speckle pattern is its output polarization. In Fig.S5.D, we report the output polarization diagram of light for three layers of parafilm. The latter is obtained by rotating a polarizer and measuring the total detected intensity. As one can see, the output polarization is very close to the input laser polarization, which means that three layers of parafilm is not thick enough to completely mix the speckle polarization.

FUNDING INFORMATION

This research has been funded by the European Research Council ERC Consolidator Grant (Grant SMARTIES - 724473). SG is a member of the Institut Universitaire de France.

REFERENCES

1. N. Garcia, A. Genack, and A. Lisyansky, "Measurement of the transport mean free path of diffusing photons," Phys. Rev. B **46**, 14475 (1992).
2. D. Contini, F. Martelli, and G. Zaccanti, "Photon migration through a turbid slab described by a model based on diffusion approximation. i. theory," Appl. optics **36**, 4587–4599 (1997).
3. N. Curry, P. Bondareff, M. Leclercq, N. F. Van Hulst, R. Sapienza, S. Gigan, and S. Grésillon, "Direct determination of diffusion properties of random media from speckle contrast," Opt. letters **36**, 3332–3334 (2011).